SUBMITTED IN PARTIAL FULFILLMENT OF THE REQUIREMENTS FOR THE DEGREE OF MECHATRONIC ENGINEER

AUTHOR: CRISTIAN ALFREDO ORELLANA CEPEDA

TUTOR: ING. CRISTINA GISELLE OSCULLO NARANJO

PROTOTYPE OF PHOTOVOLTAIC GENERATOR USING ARTIFICIAL INTELLIGENCE TO CONTROL AND OPTIMIZE THE MAXIMUM POWER POINT TRACKING

CERTIFICATE OF AUTORSHIP

I, Cristian Alfredo Orellana Cepeda, hereby declare that this submission is my own work, it has not been previously submitted for any degree or professional qualification and that the detailed bibliography has been consulted.

I transfer my intellectual property rights to the Universidad Internacional del Ecuador, to be published and divulged on the internet, according to the provisions of the Ley de Propiedad Intelectual, its regulations and other legal dispositions.

Cristian Alfredo Orellana Cepeda

ACKNOWLEDGMENTS

I would like to express my gratitude towards my parents Jhon Orellana and Isabel Cepeda, for their unwavering support and encouragement, which has helped me achieve my goals and aspirations. They were a great guide for me during the development of this project, which could not have been carried out without them.

I would like to extend my gratitude to my thesis advisor Engineer Cristina Oscullo and my thesis reader Engineer Andrea Pilco, for their invaluable guidance and feedback that enabled me to successfully complete this thesis project.

I want to express my gratitude to my entire family for having trusted in me and for giving me the support that I needed throughout this academic period. They have been my source of my inspiration, I cannot thank them enough for being there for me.

Finally, I want to thank the people who have accompanied me throughout my university journey: my friends. We have overcome all the adversities that have been presented to us together, always giving each other support, being there in the good and the bad times. It was an honor to have shared so much with you for 4 years and counting. Always grateful to Dennis, Brenda, David, Francisco, Martín, Matías, Marco. I apologize for not being able to mention everyone, this list would be endless, but each of you has left an important mark on my life. Thank you so much for having been a fundamental part of my growth and development as a person.

CONTENTS

1 Conceptual design **1**

1.1 Introduction 1

1.2 Project photovoltaic panel (PV) 3

1.3 PV rotate mechanism 4

1.4 Solar tracker prototype operation philosophy 4

1.5 Prototype schematic 5

1.6 Prototype components 6

2 Mechanical design **6**

2.1 Structure 7

2.2 Rotating mechanism design 11

3 Electronic design **23**

3.1 Electrical motor 23

3.2 Microcontroller 24

3.3 Sensors 24

3.4 Actuators 25

3.5 Electrical performance 25

3.6 Voltage storage 27

4 Computer design **27**

4.1 Artificial intelligence 27

4.2 Web interface 30

LIST OF FIGURES

1 Single-axis photovoltaic tracking systems [6] 2
2 Dual-axis photovoltaic tracking systems [6] 2
3 Solar panel YL250P-29b [10] 3
4 Classification of solar trackers according to their driving system [6] 5
5 3D prototype modeling 5
6 Isometric view of the structure 7
7 Free body diagram of the structure 8
8 Lateral view of the beam 9
9 Free body diagram of the beam 10
10 Force-moment diagram of the beam 10
11 Bosch Rexroth AG 40 × 40 profile and connectors [13] 11
12 Single enveloping gear worm [16] 12
13 Crown calculations [17] 13
14 Worm screw calculations [17] 15
15 Pitch cylinder of a worm gear [16] 16
16 Gears calculations [18] 20
17 Relation between gears 21
18 Free body diagram with dynamic loads 22
19 YL250P-29b graphs of current, power and voltage 26
20 Scatter plots of the input and output data 29
21 Heat map of the dataset 29

LIST OF TABLES

1 Solar panel YL250P-29b technical characteristics [11] 3
2 List of sensors 25
3 Energy consumption of each element 26

PROTOTYPE OF PHOTOVOLTAIC GENERATOR USING ARTIFICIAL INTELLIGENCE TO CONTROL AND OPTIMIZE THE MAXIMUM POWER POINT TRACKING

CALCULATION OF COMPONENTS AND SELECTION OF MATERIALS

The proposed solar tracker consists of mechanical, electrical and computing components, which are interrelated. The mechanical components include the structure that supports the panel and the mechanisms used. The electronic components include the microcomputer, the sensors and the actuators that control the rotating mechanisms. The entire photovoltaic power generation system corresponds to the electrical part of the project. The computer part includes the development of the artificial intelligence, as well as the development of the web interface to monitor the performance of the panel.

1 CONCEPTUAL DESIGN

Energy from the sun is an easily accessible, renewable, inexpensive and infinite resource, and fortunately Ecuador has great solar potential [1]. This country, since it is located in the equatorial zone, can get a constant solar radiation in certain points of the territory, obtaining 30 % more solar radiation than other countries [2].

Although the sun is a renewable energy source with great potential, it can only be fully exploited if the photovoltaic panels receive the sun's rays perpendicularly. So, it is essential to maximize irradiance capture with a solar tracking system. At a theoretical level, the tracking problem can be solved with the help of solar equations. However, in practice there are a number of uncertainties that are not usually taken into account, such as radiation or the environmental conditions of the day [3].

1.1 Introduction

Solar trackers can be classified according to their degrees of freedom in two types: single-axis and dual-axis trackers. The first has only one degree of freedom, with a rotation around the horizontal axis or the vertical axis. The second has two degrees of freedom, being able to rotate around both horizontal and vertical axis [4].

Single-axis trackers are usually cheap and increase energy production by 28 %, and are commonly used in latitudes close to the equator [5]. In Fig. 1, it is possible to see the three types of single-axis trackers: horizontal single-axis tracking system (HSAT), vertical single-axis tracking system (VSAT) and tilted single-axis tracking system (TSAT) [6].

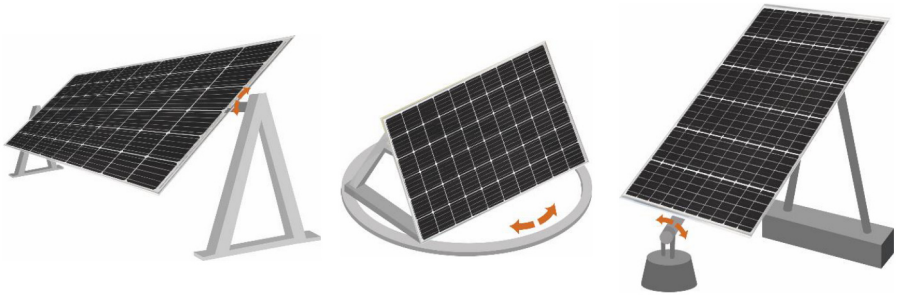

(a) HSAT (b) VSAT (c) TSAT

Figure 1: Single-axis photovoltaic tracking systems [6]

Dual-axis trackers tend to be more expensive to implement and increase production by approximately 35 % [7]. In Fig. 2 appear the two types of dual-axis trackers: tip-tilt dual-axis tracking system (TTDAT) and azimuth-altitude dual-axis tracking system (AADAT) [6].

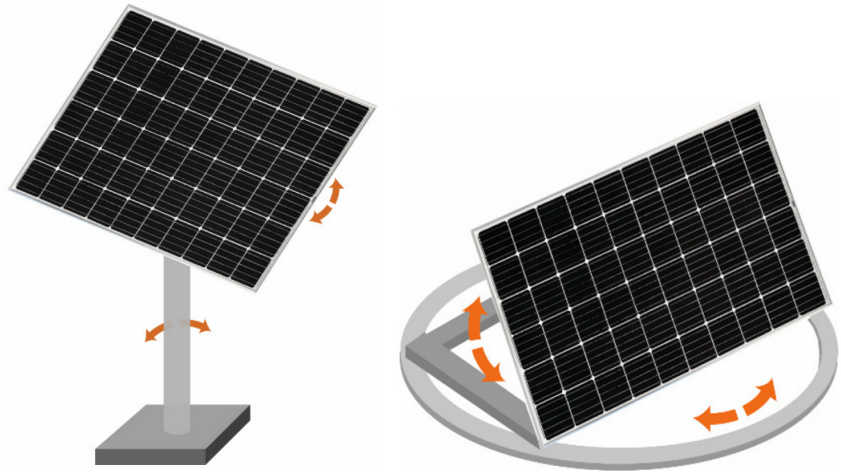

(a) TTDAT (b) AADAT

Figure 2: Dual-axis photovoltaic tracking systems [6]

The present project will be focused on a HSAT model, because Ecuador is very close to the equator. Additionally, it is the best option according to [5], [8] and [9].

1.2 Project photovoltaic panel (PV)

Once the type of tracker to be implemented has been clarified, it is important to take into account that the used solar panel is an available Yingli Solar YL250P-29b (250W) Solar Panel, like the one shown in Fig. 3.

Figure 3: Solar panel YL250P-29b [10]

The design must take into account the technical characteristics indicated in the TABLE 1.

Table 1: Solar panel YL250P-29b technical characteristics [11]

Type	Polycrystalline Silicon
Length	1650 mm (65 in)
Width	990 mm (39 in)
Depth	40 mm (1.6 in)
Weight	19.1 kg (42.1 lb)
Frame color	Clear
Output terminal type	Amphenol H4
Output cable wire gauge	12 AWG
Output cable wire type	PV Wire
Output cable wire length	1100 mm (43.3 in)
STC power rating	250 W
STC power per unit of area	14.2 W/ft² (153 W/m²)
Peak efficiency	15.3 %
Number of cells	60
STC current at maximum power point	8.24 A
STC voltage at maximum power point	30.4 V
Short-circuit current	8.79 A
Open-circuit voltage	38.4 V

1.3 PV rotate mechanism

The aim of the project is to obtain the highest possible electric efficiency. This implies that the use of a pump for hydraulic cylinders or a compressor for pneumatic cylinders to move the prototype are discarded due to its high energy consumption.

To rotate the panel in one direction, like the HSAT system, a gear mechanism and a worm screw mechanism have to be developed. The materials for them are strong enough to handle with the generated stresses. The mechanical energy required to move the worm screw must be supplied by one electrical DC motor. The torque generated by the motor must be transferred to the worm gear mechanism via a set of transmitting gears.

1.4 Solar tracker prototype operation philosophy

A solar tracker is a device which main purpose is to increase the production of electrical energy obtained from a solar panel by means of mechanical, electrical and electronic systems that follow the path of the sun. Following the sun causes its rays to fall perpendicularly on the panel, increasing the capture of solar radiation and therefore the energy generated [12]. Solar trackers can be classified according to their drive system, their degrees of freedom, as it was shown before, or their control system.

Depending on their driving system, trackers can be active or passive. Passive tracking systems use special liquids or gases with a low boiling point. They base their operation on the pressure difference of these substances, so they do not need additional power supplies. They are not very common because they are usually not as accurate. On the other hand, active trackers use electrical and mechanical systems to operate. They can be controlled by artificial intelligence or by microprocessors [6]. Both types of trackers can be seen in Fig. 4.

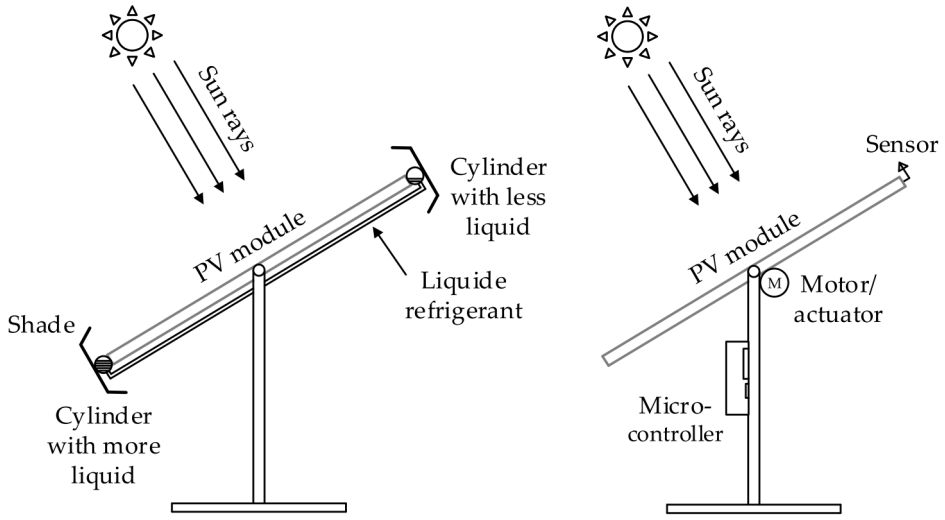

(a) Passive tracking system (b) Active tracking system

Figure 4: Classification of solar trackers according to their driving system [6]

Depending on the control system, it can be an open-loop system, a closed-loop system or a hybrid between the two types. The first uses a mathematical algorithm to determine the position that must have the solar panel so that the rays fall perpendicular to it, it is not fed back with errors that may appear. The second relies on sensor feedback and moves the axes after the sensor detects where the sun is located [6].

1.5 Prototype schematic

The proposed prototype has been modeled in 3D, as shown in Fig. 5.

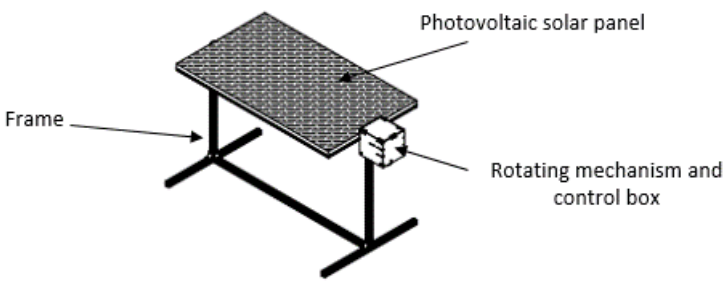

Figure 5: 3D prototype modeling

1.6 Prototype components

The proposed horizontal single-axis tracking system (HSAT) prototype has the following main components to be designed depending on the referred photovoltaic panel.

- ❒ **Mechanical components**
  - ✧ The rotation mechanism that allows the PV to rotate includes a worm gear and a set of gears.
  - ✧ Frame to support the solar panel, the rotating mechanism and the control component box.
- ❒ **Electronic components**
  - ✧ Motor DC to convert the electrical energy provided by the own photovoltaic panel into mechanical energy to rotate the PV.
  - ✧ Microcontroller to control the PV performance according with the solar incidence.
  - ✧ Sensors for electrical voltage and current, solar irradiance, pressure, humidity and temperature.
  - ✧ Actuators to allow the motor operation, such as relays and voltage regulator.
  - ✧ Battery charge to store the PV performance
- ❒ **Programming software development**
  - ✧ Artificial intelligence to determine the correct position of the PV.
  - ✧ Python routines programming.
  - ✧ Web interface.

2 MECHANICAL DESIGN

Next, the calculation of the components and the selection of materials for each of them is carried out. To design the rotation mechanism and the prototype frame, it is necessary to calculate the principal stresses and the maximum moment exerted by the panel during its horizontal rotation.

2.1 Structure

The frame should support the photovoltaic panel, the rotating mechanism and electronic elements. It is mostly designed from stiffness considerations and thus should possess high static and dynamic stiffness.

Since the structure will be in constant movement and will be exposed to the weather, the material must not be too heavy and it must withstand extreme environmental conditions. Additionally, due to the dynamism that is intended to have and for cost reasons, the structure should not be completely solid. This indicates that the most suitable material to work with are aluminum profiles.

The flexible and modular mounting system from manufacturer Bosch Rexroth offers fast and comprehensive solutions for several applications. The modular system is based on aluminum profiles with an "endless" longitudinal groove [13].

2.1.1 Stress and momentum calculation

Fig. 6, shows the isometric view of the structure that will support the panel. For the calculation, the red-enclosed right vertical column will be chosen because the component box will be located there, so it will support more loads than its counterpart, and if the chosen profile supports them, the other column will. The length of that column is $0.93\,\mathrm{m}$

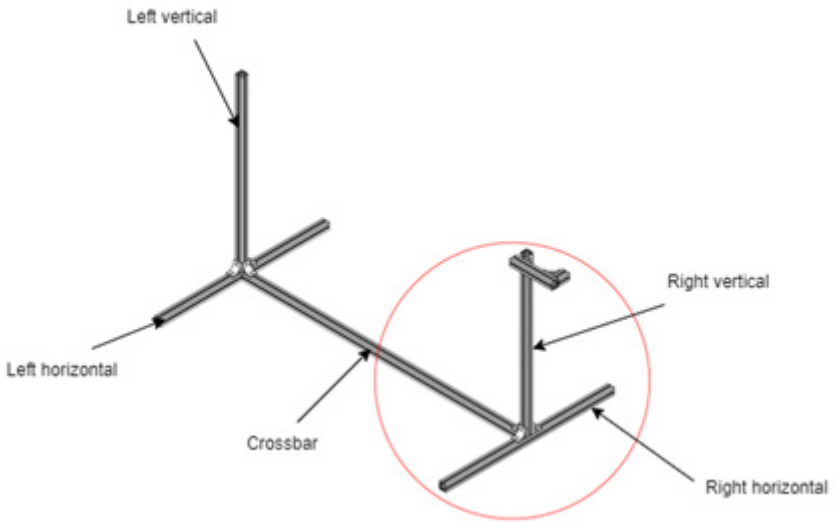

Figure 6: Isometric view of the structure

Free body diagram

To begin with, the free body diagram of the right vertical column must be analyzed, as shown in Fig. 7. The force F represents the half of the panel weight, because it will be distributed in both columns. The force C is the box weight, including all the electronic components and the entire case. The moment M_M represents the necessary torque in order to rotate the solar panel. All the stresses will be calculated around the point P, so there are a reaction force R_P and a moment M_P.

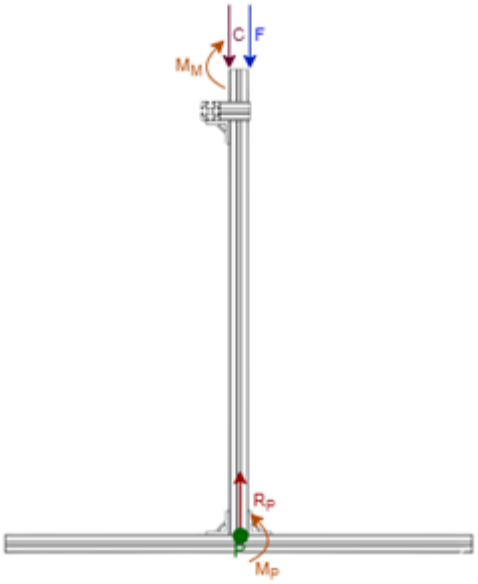

Figure 7: Free body diagram of the structure

Force analysis

Checking TABLE 1, the panel has a weight of 19.1 kg, and the box has a weight of 1 kg.

$$F = \left(\frac{19.1\,\mathrm{kg}}{2}\right)(9.81\,\mathrm{m/s^2}) = 93.69\,\mathrm{N}$$

$$C = (1\,\mathrm{kg})(9.81\,\mathrm{m/s^2}) = 9.81\,\mathrm{N}$$

$$\sum F = 0$$

$$R_P - F - C = 0$$

$$R_P = 93.69\,\mathrm{N} + 9.81\,\mathrm{N} = 103.5\,\mathrm{N}$$

Considering that the yield strength of aluminium 6061-T4 is 145 MPa, its modulus of elastic-

ity is 68.9 GPa [14], and that it is assumed a safety factor of 10 due to any eventuality, it is possible to get the following results for normal stress and bucking.

Normal stress

$$\sigma = f_s \left(\frac{R_P}{A} \right) \rightarrow A = \frac{R_P}{\frac{\sigma}{f_s}}$$

$$A = \frac{103.5\,\mathrm{N}}{\frac{145 \times 10^6\,\mathrm{Pa}}{10}} = 7.14 \times 10^{-6}\,\mathrm{m}^2 = 7.14\,\mathrm{mm}^2$$

Bucking

$$P_{cr} = \frac{\pi^2 EI}{f_s L^2} \rightarrow I = \frac{P_{cr} f_s L^2}{\pi^2 E}$$

$$I = \frac{(103.5\,\mathrm{N})(10)(0.93\,\mathrm{m})}{\pi^2 (68.9 \times 10^9\,\mathrm{Pa})} = 1.41542 \times 10^9\,\mathrm{m}^4 = 1415.42\,\mathrm{mm}^4$$

Considering the availability in the market, the aluminium profile Bosch Rexroth AG 40 × 40 was chosen. Its cross-sectional area is 560 mm^2 and their second moments of area I_x and I_y are both 91000 mm^4 [13]. Both the cross-sectional area and the second moments of area are enough for the application.

Maximum moment

The frame of the panel is composed by rectangular profiles 0.92 m long 0.02 m wide and 0.02 m thick. It is possible to determine the rotational inertia in the center of mass, the black dot in Fig. 8.

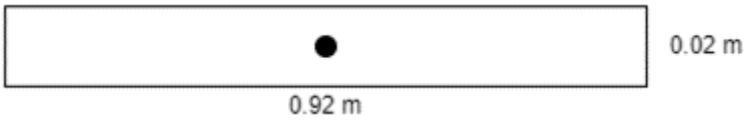

Figure 8: Lateral view of the beam

The weight of the solar panel could be determine with the following expression:

$$P = (19.1\,\mathrm{kg})(9.81\,\mathrm{m/s^2}) = 187.37\,\mathrm{N}$$

The solar panel exerts a distributed load over the beam equivalent to its weight, as it can be seen in Fig. 9. It is important to remark that the support point is located at the center of

gravity, the black dot of the diagram. There will appear a moment M_V and a reaction force F_V, that will be calculated later.

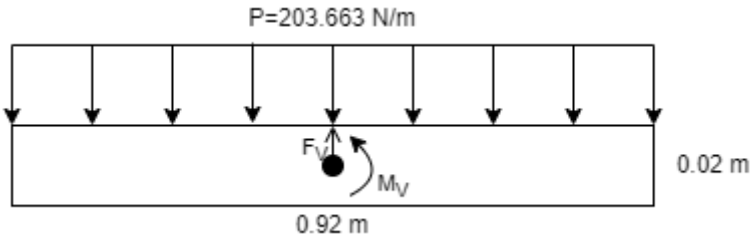

Figure 9: Free body diagram of the beam

$$F_V = P = 187.37\,\mathrm{N}$$

The force-moment diagram is shown in Fig. 10. There it can be seen that the maximum moment is 43.10 N · m and the maximum force is 93.69 N.

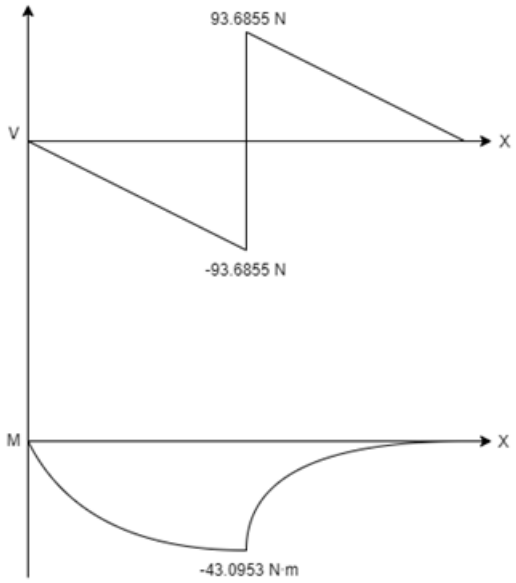

Figure 10: Force-moment diagram of the beam

2.1.2 Structural material selection

The selected material for the frame prototype, considering the previous calculations, is aluminum profile Bosch Rexroth AG 40 × 40, with related joints and connections elements. Fig. 11 shows a modular Bosch Rexroth profile and connectors type.

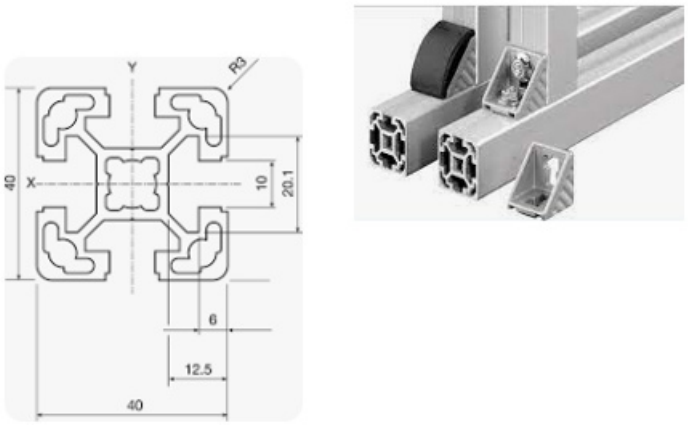

Figure 11: Bosch Rexroth AG 40 × 40 profile and connectors [13]

2.2 Rotating mechanism design

It is important to determine the necessary torque to rotate the solar panel. Notice that the torque must be greater than the maximum moment obtained before in the graph, so let assume τ as 50 N · m.

First of all, it is necessary to check whether the motor shaft is able to withstand the stresses exerted on it. Considering a steel AISI 1040 for the motor shaft, with a 5-mm radius, and a 50-mm length, and that the half of the panel weight is acting over it, the critical load will be the following:

$$A = \pi R^2$$

$$A = \pi(0.005\,\mathrm{m})^2 = 7.854 \times 10^{-5}\,\mathrm{m}$$

$$I = \frac{\pi R^4}{4}$$

$$I = \frac{\pi(0.005\,\mathrm{m})^4}{4} = 4.9087 \times 10^{-10}\,\mathrm{m}^4$$

$$T_x = (5 \times 10^{-3}\,\mathrm{m})(9.81\,\mathrm{m/s^2})(9.55\,\mathrm{kg}) = 0.4684\,\mathrm{N \cdot m}$$

$$M_y = (50 \times 10^{-3}\,\mathrm{m})(9.81\,\mathrm{m/s^2})(9.55\,\mathrm{kg}) = 4.6842\,\mathrm{N \cdot m}$$

$$\sigma = \frac{M_y C}{I}$$

$$\sigma = \frac{(4.6842\,\mathrm{N \cdot m})(5 \times 10^{-3}\,\mathrm{m})}{4.9087 \times 10^{-10}\,\mathrm{m}^4} = 47.7132\,\mathrm{MPa}$$

The yield strength of the AISI 1040 steel is 415 MPa [15], so it is correct to conclude that it is enough to support the 50 MPa generated by the panel. However, due to ambient factors, such as wind or rain, the panel tends to move, behavior that is bad for the project. For this issue, it is necessary to implement a single gear worm mechanism, like the one in Fig. 12, which is an one-way mechanism, avoiding disturbances.

Figure 12: Single enveloping gear worm [16]

The torque generated by the electrical motor must be transferred to the worm gear mechanism via a set of gears.

2.2.1 Gear worm calculations

The gear worm mechanism consisted of the crown and endless screw

Crown calculations

To develop this design, it is required to set the number of teeth N and the external diameter D_e. Due to the limited space, it is desired 42 teeth and an 88 mm external diameter. In the following equations, M represents the module, D_p is the pitch diameter, P is the pitch, H is the height of the teeth, D_1 is the major diameter, A is the wheel width, R is the peripheral concavity and r is the head radius. Fig. 13 shows graphically these parameters.

$$M = \frac{D_e}{N+2}$$

$$M = \frac{88\,\mathrm{mm}}{42+2} = 2\,\mathrm{mm}$$

$$D_p = M(N)$$

$$D_p = 2\,\mathrm{mm}(42) = 84\,\mathrm{mm}$$

$$P = \pi M$$

$$P = \pi(2\,\mathrm{mm}) = 6.2832\,\mathrm{mm}$$

$$H = 2.167M$$

$$H = 2.167(2\,\mathrm{mm}) = 4.334\,\mathrm{mm}$$

$$D_1 = D_e + 0.4775P$$

$$D_1 = 88\,\mathrm{mm} + 0.4775(6.2832\,\mathrm{mm}) = 91\,\mathrm{mm}$$

$$A = 6 + 2.38P$$

$$A = 6 + 2.38(6.2832\,\mathrm{mm}) = 20.954\,\mathrm{mm}$$

$$R = 0.5D_p - M$$

$$R = 0.5(84\,\mathrm{mm}) - 2\,\mathrm{mm} = 40\,\mathrm{mm}$$

$$r = 0.25P$$

$$r = 0.25(6.2832\,\mathrm{mm}) = 1.5708\,\mathrm{mm}$$

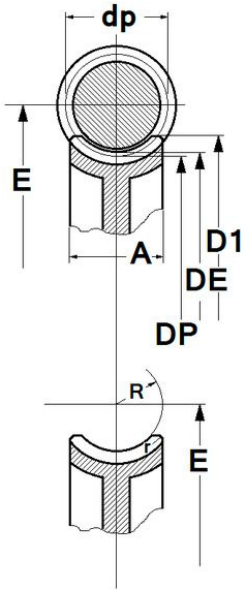

Figure 13: Crown calculations [17]

Endless screw calculations

For the calculations, a 2 mm module M and the number of entries as 1 are considered, for a β of 14º30'. In the following equations, P is the pitch, D_p represents the pitch diameter, H is the height of the teeth, D_e is the external diameter, D is the internal diameter, α is the fillet

angle, e is the fillet thickness, c represents the fillet spacing, l is the tooth foot height, T is the fillet bottom width, LR is the threaded part length, F represents the non-threaded length, the head radius is r and the distance between centers is E. Fig. 14 shows graphically these parameters.

$$P = \pi M$$

$$P = \pi(2\,\mathrm{mm}) = 6.2832\,\mathrm{mm}$$

$$H = 2.167M$$

$$H = 2.167(2\,\mathrm{mm}) = 4.334\,\mathrm{mm}$$

$$D_p = 10M$$

$$D_p = 10(2\,\mathrm{mm}) = 20\,\mathrm{mm}$$

$$D_e = D_p + 2M$$

$$D_e = 20\,\mathrm{mm} + 2(2\,\mathrm{mm}) = 24\,\mathrm{mm}$$

$$D = D_e - 2H$$

$$D = 24\,\mathrm{mm} - 2(4.334\,\mathrm{mm}) = 15.332\,\mathrm{mm}$$

$$\alpha = \arctan(\frac{nM}{D_p})$$

$$\alpha = \arctan\left(\frac{1(2\,\mathrm{mm})}{20\,\mathrm{mm}}\right) = 5.7106^\circ$$

$$e = \frac{P}{2}$$

$$e = \frac{6.2832\,\mathrm{mm}}{2} = 3.1416\mathrm{mm}$$

$$c = \frac{P}{2}$$

$$c = \frac{6.2832\,\mathrm{mm}}{2} = 3.1416\mathrm{mm}$$

$$l = M$$

$$l = 2\,\mathrm{mm}$$

$$T = \left(\frac{P \arctan(\beta)}{4} - l \right) (2 \tan(\beta))$$

$$T = \left(\frac{(2\,\mathrm{mm}) \arctan(14°30')}{4} - 2\,\mathrm{mm} \right) (2 \tan(14°30')) = 2.1071\,\mathrm{mm}$$

$$LR = P \left(4.5 + \frac{N}{50} \right)$$

$$LR = 6.2832\,\mathrm{mm} \left(4.5 + \frac{42}{50} \right) = 33.5522\,\mathrm{mm}$$

$$F = P$$

$$F = 6.2832\,\mathrm{mm}$$

$$r = 0.05P$$

$$r = 0.05(6.2832\,\mathrm{mm}) = 0.3142\,\mathrm{mm}$$

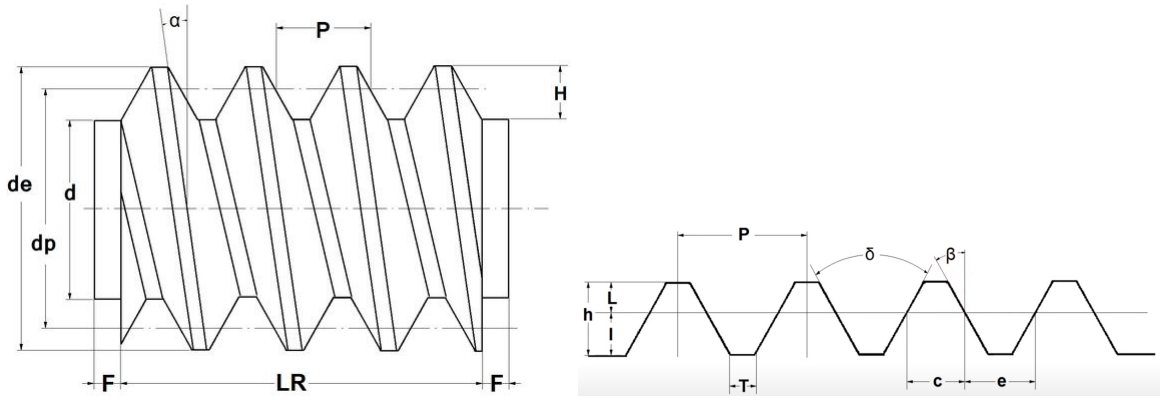

(a) Thread (b) Teeth

Figure 14: Worm screw calculations [17]

Once the mechanism is designed, the dynamics must be analyzed. In this case, neither strength nor speed change because there is no increment in the number of teeth or the diametrical length. Additionally, the transmission losses are lower than the 2%, so they are negligible.

It is required to verify if the input forces sum minus the weight of the system is positive. First, it is necessary to determine the efficiency, checking the equation where η is the efficiency, f is the coefficient of friction, λ is the helix angle and ϕ is the fillet angle, as it can be seen in Fig. 15.

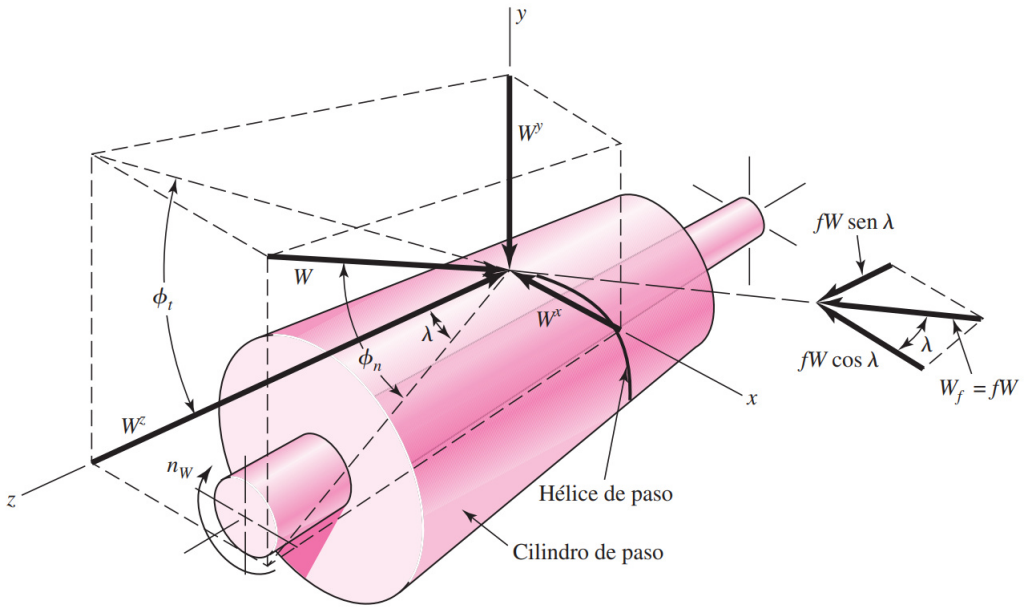

Figure 15: Pitch cylinder of a worm gear [16]

To calculate the efficiency, it is possible to check the following expression:

$$\eta = \frac{\cos(\phi) - f\tan(\lambda)}{\cos(\phi) + f\cot(\lambda)}$$

$$\eta = \frac{\cos(5.71°) - (0.78)\tan(14.3°)}{\cos(5.71°) + (0.78)\cot(14.3°)} = 0.711$$

As it can be seen, the friction affects the transmission, reducing it a 28.9 %. Now, for the forces decomposition will be determined in the following expressions, taking into account the graph shown in Fig. 15. W^x, W^y, W^z are the decomposed forces in their three axis.

$$W^x = W(\cos(\phi)\sin(\lambda) + f\cos(\lambda))$$

$$W^y = W\sin(\phi)$$

$$W^z = W(\cos(\phi)\cos(\lambda) - f\sin(\lambda))$$

In this case, to calculate the forces, the torque T and the pitch diameter D are set respectively as 50 N · m and 95 mm, as it was mentioned before. And, the torque T to break the inertia is 43.09 N · m.

$$W_1 = \frac{T}{D}$$

$$W_1 = \frac{50\,\mathrm{N}\cdot\mathrm{m}}{95\times10^{-3}\,\mathrm{m}} = 526.3158\,\mathrm{N}$$

$$W_2 = \frac{T}{D}$$

$$W_2 = \frac{43.0953\,\mathrm{N}\cdot\mathrm{m}}{95\times10^{-3}\,\mathrm{m}} = 453.6347\,\mathrm{N}$$

It is important to determine their components with the equations shown before, according to the stresses generated over the worm screw.

$$W_1^x = 526.3158\,\mathrm{N}(\cos(5.71^\circ)\sin(14.3^\circ) + 0.78\cos(14.3^\circ)) = 527.1609\,\mathrm{N}$$

$$W_1^y = 526.3158\,\mathrm{N}\sin(5.71^\circ) = 52.365\,\mathrm{N}$$

$$W_1^z = 526.3158\,\mathrm{N}(\cos(5.71^\circ)\cos(14.3^\circ) + 0.78\sin(14.3^\circ)) = 608.8773\,\mathrm{N}$$

$$W_2^x = 453.6347\,\mathrm{N}(\cos(5.71^\circ)\sin(14.3^\circ) + 0.78\cos(14.3^\circ)) = 454.3631\,\mathrm{N}$$

$$W_2^y = 453.6347\,\mathrm{N}\sin(5.71^\circ) = 45.1337\,\mathrm{N}$$

$$W_2^z = 453.6347\,\mathrm{N}(\cos(5.71^\circ)\cos(14.3^\circ) + 0.78\sin(14.3^\circ)) = 524.795\,\mathrm{N}$$

Now, it is time to evaluate every axis and the forces that act over them.

$$\sum F_x = W_R^x$$

$$W_1^x - W_2^x = W_R^x$$

$$W_R^x = 527.1609\,\mathrm{N} - 454.3631\,\mathrm{N} = 72.7978\,\mathrm{N}$$

$$\sum F_y = W_R^y$$

$$W_1^y - W_2^y = W_R^y$$

$$W_R^y = 52.365\,\mathrm{N} - 45.1337\,\mathrm{N} = 7.2313\,\mathrm{N}$$

$$\sum F_z = W_R^z$$

$$W_1^z - W_2^z = W_R^z$$

$$W_R^z = 608.8773\,\mathrm{N} - 524.795\,\mathrm{N} = 84.0823\,\mathrm{N}$$

$$W_R = \sqrt{W_R^{x\,2} + W_R^{y\,2} + W_R^{z\,2}}$$

$$W_R = \sqrt{(72.7978\,\mathrm{N})^2 + (7.2313\,\mathrm{N})^2 + (84.0823\,\mathrm{N})^2} = 111.4524\,\mathrm{N}$$

Once the resultant force is positive, this will be able to move the system without problems.

2.2.2 Gears calculations

Since they are not going to vary torque and speed, it is desired a transmission ratio i of 1, implying that both pinion and wheel have the same number of teeth. However, due to the space, the pinion will have 19 teeth (z_2) and the wheel will have 18 teeth (z_3). Additionally, the module m will be 5 mm because of the manufacturing process, which is 3D-printing. With this data, it is possible to get the other design parameters for the gears, such as the tooth head height h_a, the tooth foot height h_f, the pinion and wheel pitch diameters (d_2, d_3), the distance between centers a, the external diameter for the pinion an wheel (d_{e_2}, d_{e_3}), the internal diameter for the pinion and wheel (d_{e_2}, d_{e_3}), the tooth thickness s, the tooth gap width s', the pitch p, the notch radius r, the pressure angle of the pinion and wheel (α_2, α_3) and the angle between teeth of the pinion an wheel (β_2, β_3). These parameters can be seen in Fig. 16.

$$h_a = m$$

$$h_a = 5\,\mathrm{mm}$$

$$h_f = 1.25m$$

$$h_f = 1.25(5\,\mathrm{mm}) = 6.25\,\mathrm{mm}$$

$$d_2 = z_2 m$$

$$d_2 = 19(5\,\text{mm}) = 95\,\text{mm}$$

$$d_3 = z_3 m$$

$$d_3 = 18(5\,\text{mm}) = 90\,\text{mm}$$

$$a = \frac{d_2 + d_3}{2}$$

$$a = \frac{95\,\text{mm} + 90\,\text{mm}}{2} = 92.5$$

$$i = \frac{z_2}{z_3}$$

$$i = \frac{19}{18} = 1.06$$

$$d_{e_2} = d_2 + 2h_a$$

$$d_{e_2} = 95\,\text{mm} + 2(5\,\text{mm}) = 105\,\text{mm}$$

$$d_{e_3} = d_3 + 2h_a$$

$$d_{e_3} = 90\,\text{mm} + 2(5\,\text{mm}) = 100\,\text{mm}$$

$$d_{i_2} = d_2 - 2h_f$$

$$d_{i_2} = 95\,\text{mm} - 2(6.25\,\text{mm}) = 82.5\,\text{mm}$$

$$d_{i_3} = d_3 - 2h_f$$

$$d_{i_3} = 90\,\text{mm} - 2(6.25\,\text{mm}) = 77.5\,\text{mm}$$

$$s = \frac{19}{40} m\pi$$

$$s = \frac{19}{40}(5\,\text{mm})\pi = 7.4613\,\text{mm}$$

$$s' = \frac{21}{40} m\pi$$

$$s' = \frac{21}{40}(5\,\text{mm})\pi = 8.2467\,\text{mm}$$

$$p = m\pi$$

$$p = (5\,\text{mm})\pi = 15.708\,\text{mm}$$

$$r = \frac{p}{12}$$

$$r = \frac{15.708\,\text{mm}}{12} = 1.309\,\text{mm}$$

$$\alpha_2 = \arccos\left(\frac{\frac{d_{i_2}}{2}}{\frac{d_2}{2}}\right)$$

$$\alpha_2 = \arccos\left(\frac{\frac{82.5\,\text{mm}}{2}}{\frac{95\,\text{mm}}{2}}\right) = 29.7243^\circ$$

$$\alpha_3 = \arccos\left(\frac{\frac{d_{i_3}}{2}}{\frac{d_3}{2}}\right)$$

$$\alpha_3 = \arccos\left(\frac{\frac{77.5\,\text{mm}}{2}}{\frac{90\,\text{mm}}{2}}\right) = 30.5584^\circ$$

$$\beta_2 = \frac{360}{z_2}$$

$$\beta_2 = \frac{360}{19} = 18.9474^\circ$$

$$\beta_3 = \frac{360}{z_3}$$

$$\beta_3 = \frac{360}{18} = 20^\circ$$

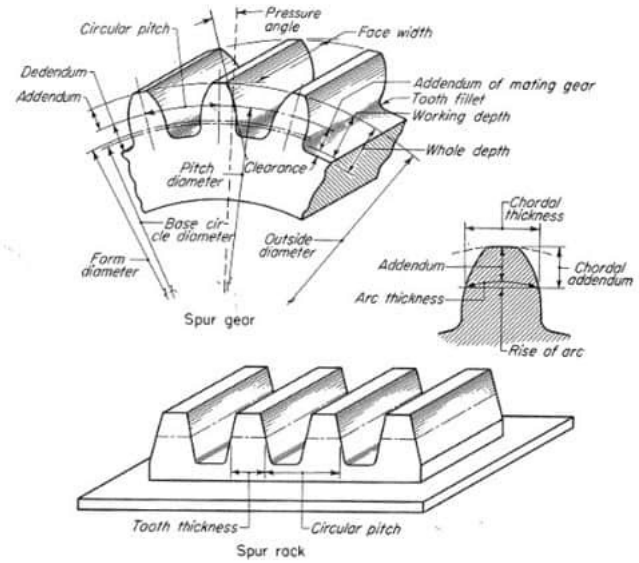

Figure 16: Gears calculations [18]

Once the values were determined, it is time to calculate the generated stresses to check if the material is strong enough to support them. For this, considering that the pinion has a

95 mm diameter, as it can be seen in Fig. 17, working at 60 rpm, and transmitting 60 W to the wheelat a pressure angle α of 30º, it is possible to get the tangential and radial forces applied from the pinion to the wheel (F_{23}^t, F_{23}^t), the total force F_{23} and stress σ.

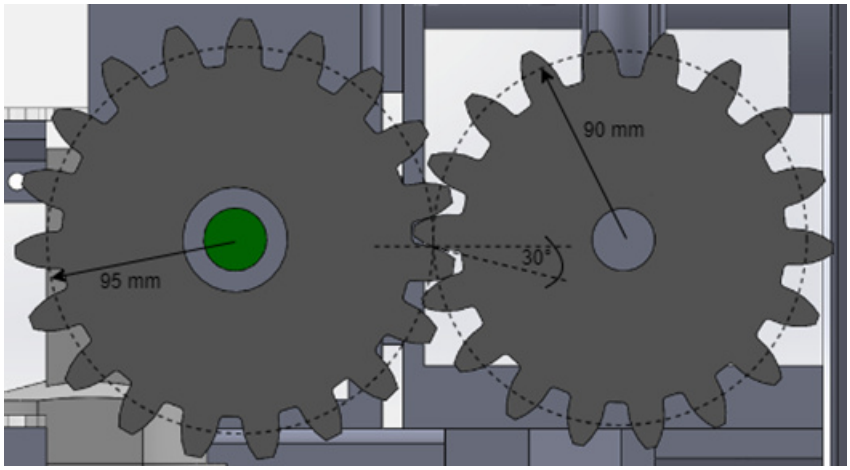

Figure 17: Relation between gears

$$F_{23}^t = \frac{60000H}{\pi d_2 n}$$

$$F_{23}^t = \frac{60000(60\,\mathrm{W})}{\pi(95\,\mathrm{mm})(60\,\mathrm{rpm})} = 201.0378\,\mathrm{N}$$

$$F_{23}^r = F_{23}^t \tan(\alpha)$$

$$F_{23}^r = 201.0378\,\mathrm{N}\tan(30^\circ) = 116.0692\,\mathrm{N}$$

$$F_{23} = \sqrt{{F_{23}^t}^2 + {F_{23}^r}^2}$$

$$F_{23} = \sqrt{(201.0378\,\mathrm{N})^2 + (116.0692\,\mathrm{N})^2} = 232.1384\,\mathrm{N}$$

$$\sigma = \frac{F_{23}^t}{mbY}$$

$$\sigma = \frac{201.0378\,\mathrm{N}}{(5\,\mathrm{mm})(7.4613\,\mathrm{mm})(0.309)} = 17.4695\,\mathrm{MPa}$$

2.2.3 Rotating mechanism material selection

For the project it is considered the use of the Polylactic acid (PLA) material for the rotating mechanism elements. The PLA is a type of plastic that is used in building models and prototypes of solid objects and components. It is a thermoplastic polyester that serves as

the raw material in 3D printing or additive manufacturing processes and applications [19].

Considering that the PLA has a yield strength of 55 MPa, and the generated stress by the gears is 17.47 MPa, it is possible to conclude that this material is strong enough for this mechanism. This was the static analysis.

For the dynamic analysis, it is required to determine if the exerted force is able to break the inertia of the system. As it was mentioned before, the desired motion ratio is almost unitary, so it is assumed to be 1. The dynamic forces between the gears are the ones shown in Fig. 18.

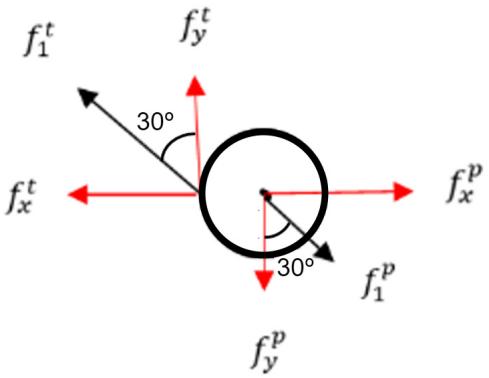

Figure 18: Free body diagram with dynamic loads

$$f_1^t = W_1$$

$$f_y^t = f_1^t \cos(\alpha)$$

$$f_y^t = 526.3158\,\mathrm{N}\cos(30^\circ) = 455.8029\,\mathrm{N}$$

$$f_x^t = f_1^t \sin(\alpha)$$

$$f_x^t = 526.3158\,\mathrm{N}\sin(30^\circ) = 263.1579\,\mathrm{N}$$

$$f_1^p = W_2$$

$$f_y^p = f_1^p \cos(\alpha)$$

$$f_y^p = 453.6347\,\mathrm{N}\cos(30^\circ) = 392.8592\,\mathrm{N}$$

$$f_x^p = f_1^p \sin(\alpha)$$

$$f_x^p = 453.6347\,\mathrm{N}\sin(30^\circ) = 223.8174\,\mathrm{N}$$

$$\sum F_x = F_{R_x}$$

$$f_x^t - f_x^p = F_{R_x}$$

$$F_{R_x} = 263.1579\,\mathrm{N} - 223.8174\,\mathrm{N} = 39.3405\,\mathrm{N}$$

$$\sum F_y = F_{R_y}$$

$$f_y^t - f_y^p = F_{R_y}$$

$$F_{R_y} = 455.8029\,\mathrm{N} - 392.8592\,\mathrm{N} = 62.9437\,\mathrm{N}$$

$$F_R = \sqrt{{F_{R_x}}^2 + {F_{R_y}}^2}$$

$$F_R = \sqrt{(39.3405\,\mathrm{N})^2 + (62.9437\,\mathrm{N})^2} = 74.2266\,\mathrm{N}$$

$$F_T^C = f_1^t + f_1^p$$

$$F_T^C = 526.3158\,\mathrm{N} + 453.6347\,\mathrm{N} = 979.9505\,\mathrm{N}$$

Considering that the minimum pressure area of the gear is 1 cm^2, it is possible to determine the stress with the compression total force F_T^C.

$$\sigma = \frac{979.9505\,\mathrm{N}}{1\,\mathrm{cm}^2} = 9.7995\,\mathrm{MPa}$$

Considering this, it is possible to conclude that the gears will be strong enough, because its yield strength is 55 MPa.

3 ELECTRONIC DESIGN

3.1 Electrical motor

When selecting a motor, the first thing to consider is what the rotational speed is and what the required torque of the motor will be.

Since the photovoltaic panel should be horizontal rotation slowly, assumed a rotational speed maximum of 5 rpm. The mechanical torque was calculated in 50 N · m.

The electrical power obeys the following relationship, where P is the power, V is the voltage,

I is the current and $\cos(\phi)$ is the power factor:

$$P = \sqrt{3} V I \cos(\phi)$$

The mechanical power obeys the following relationship, where T is the torque, the motor's ability to turn loads, and n is the speed in revolutions per minute:

$$P = T \frac{n}{9.550}$$

Assuming a power factor of 85% and current of 2 amperes, the final results are the following:

$$P = (50\,\mathrm{N \cdot m}) \frac{5\,\mathrm{rpm}}{9.550} = 26.18\,\mathrm{W}$$

$$V = \frac{26.18\,\mathrm{W}}{\sqrt{3}(2\,\mathrm{A})(0.85)} = 8.90\,\mathrm{V}$$

So, for the project is selected an electrical motor of 12 V, 50 rpm, 60 W DC motor, that is more than enough according to the calculations.

3.2 Microcontroller

Since an artificial intelligence algorithm is to be implemented, we are looking to work with a Raspberry Pi, since it has support for installing all the required libraries and consists of the Python programming language. It has some input and output pines for any sensor or actuator if desired.

3.3 Sensors

TABLE 2 shows the sensors that are implemented in the system. As it can be noticed, there are four main variables that are wanted to be measured for an automatic control. The problem with these is that all their outputs are analog, and Raspberry Pi has no reading ports for them. For this reason, it is intended to use an intermediary that allows the reading of the sensors, such as the ESP32. The usage of this additionally microcontroller reduces the

project cost because it replaces all the ADCs required for the sensors. ESP32 communicates via serial port to Raspberry Pi.

Table 2: List of sensors

Variable	Sensor	Voltage
Irradiance	GYML8511	2.7 V to 5.5 V
Atmospheric pressure	BMP180	1.7 V to 3.6 V
Humidity and temperature	DHT11	1.8 V to 3.6 V

3.4 Actuators

As it was explained before, the motor that is implemented in the prototype is a 12 V, 50 rpm, 60 W DC motor. This actuator will be the one to rotate the solar panel.

On the other hand, there are some relays that will connect or disconnect some elements on the main circuit, mainly for measuring data with the sensors, in order to avoid noise.

3.5 Electrical performance

In this subsection, it will be analyzed the electrical behavior of the system, considering its energy consumption and generation.

In TABLE 3 is shown the amount of energy consumed by each element per hour. There are few elements that there were not considered in this because their consumption is negligible. As it can be seen, the device that consumes the most is the Raspberry Pi 3 B+, even though the motor requires 2 A for its function. This is because the motor is just connected for few seconds, compared to the hour that the Raspberry Pi is turned on. It is possible to conclude that the entire system has a total energetic consumption of 4.0216 Wh, consuming 96.5174 Wh-day because the system will be turned on during 24 hours.

TABLE 1 shows the electric characteristics of the solar panel. This data is used to determine the electric generation of the solar panel, obtained experimentally by the manufacturer. To get this information, they tested the panel under standard test conditions (STC): irradiance of 1000 W/m² at 25 ºC [20]. In Fig. 19 is shown the main data in a graphical way.

Table 3: Energy consumption of each element

Element	Current [A]	Time of use [h]	Charge [Ah]	Voltage [V]	Energy [Wh]
Motor	2	0.003	0.006	12	0.072
Relays	0.48	0.001	0.00048	5	0.0024
Voltage regulator	0.002	1	0.002	12	0.024
Battery charger	0.005	1	0.005	12	0.06
Current sensor	0.03	1	0.03	3.3	0.099
Irradiance sensor	0.0003	1	0.0003	5	0.0015
Pressure sensor	0.000032	1	0.000032	5	0.00016
Humidity sensor	0.0025	1	0.0025	5	0.0125
ESP32	0.15	1	0.15	5	0.75
Raspberry Pi 3 B+	0.6	1	0.6	5	3

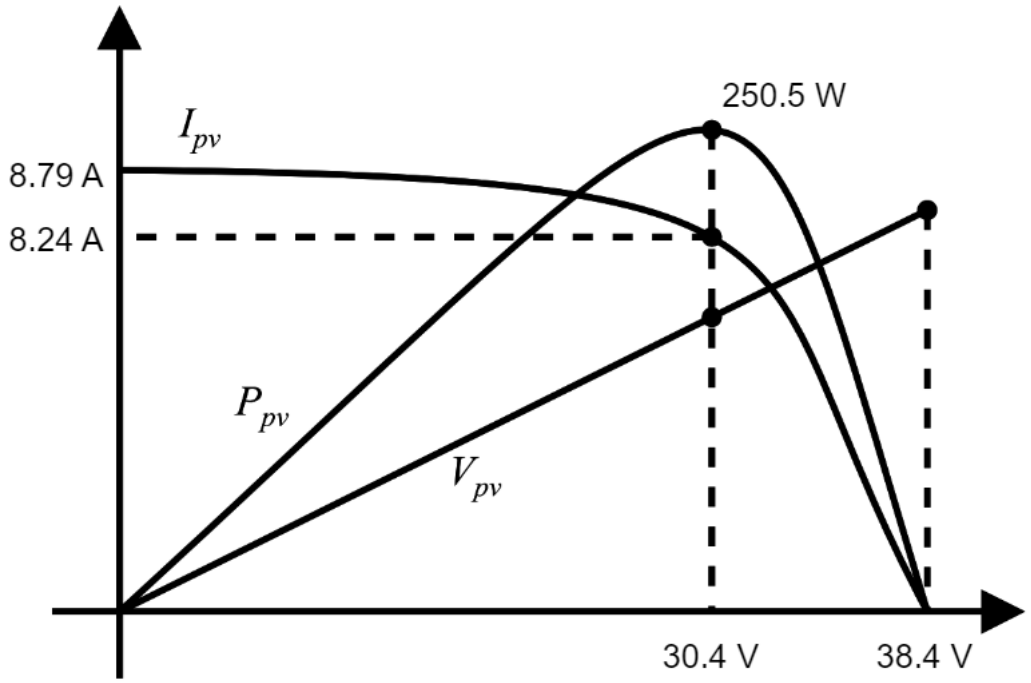

Figure 19: YL250P-29b graphs of current, power and voltage

It is possible to determine the generation considering STC, assuming that N_G is the nominal generation, R_{in} is the incident irradiance, P_l is the panel length, P_w is the panel width, P_a is the incidence area, and η is the efficiency, P_G is the generated power. Both P_l and P_w can be get from TABLE 1.

$$R_{in} = 1000\,\mathrm{W/m^2}$$

$$N_G = 250\,\mathrm{W}$$

$$P_a = P_l P_w$$

$$P_a = (1.65\,\mathrm{m})(0.99\,\mathrm{m}) = 1.6335\,\mathrm{m}^2$$

$$P_G = R_{in} P_a$$

$$P_G = (1000\,\mathrm{W/m}^2)(1.6335\,\mathrm{m}^2) = 1633.5\,\mathrm{W}$$

$$\eta = \frac{N_G}{P_G}$$

$$\eta = \frac{250\,\mathrm{W}}{1633.5\,\mathrm{W}} = 15.3045\,\%$$

3.6 Voltage storage

To store the voltage, it is desired to attach a 3 × 3 lithium battery array, via a serial-parallel connection. Each battery, with a nominal voltage of 3.7 V, is able to store 2200 mAh. Considering this, the total storage can be calculated as follows:

$$B_V = 3.7\,\mathrm{V}$$

$$B_C = 2.2\,\mathrm{Ah}$$

Serial connection: $V_T = (3.7\,\mathrm{V})(3) = 11.1\,\mathrm{V}$

Parallel connection: $C_T = (2.2\,\mathrm{Ah})(3) = 6.6\,\mathrm{Ah}$

$$T_E = (11.1\,\mathrm{V})(6.6\,\mathrm{Ah}) = 73.26\,\mathrm{Wh}$$

4 COMPUTER DESIGN

4.1 Artificial intelligence

Tests were carried out with each of the different types of possible algorithms and it was concluded that the optimal one was the neural networks. For its implementation, it was required to work with Python and the TensorFlow module. In this case, it is a multi-target algorithm, in which a set of features leads to three different outputs. This methodology

requires a few computational resources compared to the one that implies the usage of three different algorithms, each for one particular output.

On one hand, as inputs, the ambient data of the city, such as temperature, radiation, humidity and atmospheric pressure, was get from the “Secretaría del Ambiente del Municipio del Distrito Metropolitano Quito” official website in [21]. This dataset contains measures from February 2007 to March 2022, taken each hour everyday, getting a total of 132407 rows, enough for the application.

On the other hand, as outputs, the azimuth and elevation angles since 2007 were taken from [22]. This website helps to determine the sun position in every world location, so this information was filtered just for Ecuador. These angles also were used to get the actual inclination of the panel m, as it can be seen in (1), where e and a represent the elevation and azimuth angles respectively, and n is the number of the actual element in the array.

$$m_n = \begin{cases} e_n & a_n \leq 200 \\ \\ e_n - e_{n+1} + m_{n-1} & a_n > 200 \end{cases} \tag{1}$$

In Fig. 20 is shown the scatter plots of the dataset, relating two variables independent from the others. This graphs help to check which is the relation between outputs and inputs. For this project, even though there is a high dispersion in the points, it is possible to see linear and nonlinear relationships. This conclusion is supported by the heat map shown in 21, in which it is possible to see that almost every output has a negative or positive relation higher than 0.5, the only exception being elevation versus atmospheric pressure, with 0.17 points.

After the previous analysis, and bearing in mind that the database consists in four inputs and three outputs, a multioutput neural network was designed for the prediction. The proposed architecture for the implementation consists in an input layer with 5 neurons, 3 hidden layers with 100 neurons each, and an output layer with 3 neurons. This provides a 0.88, 0.86 and 0.92 accuracy for the elevation, azimuth and panel inclination angles respectively.

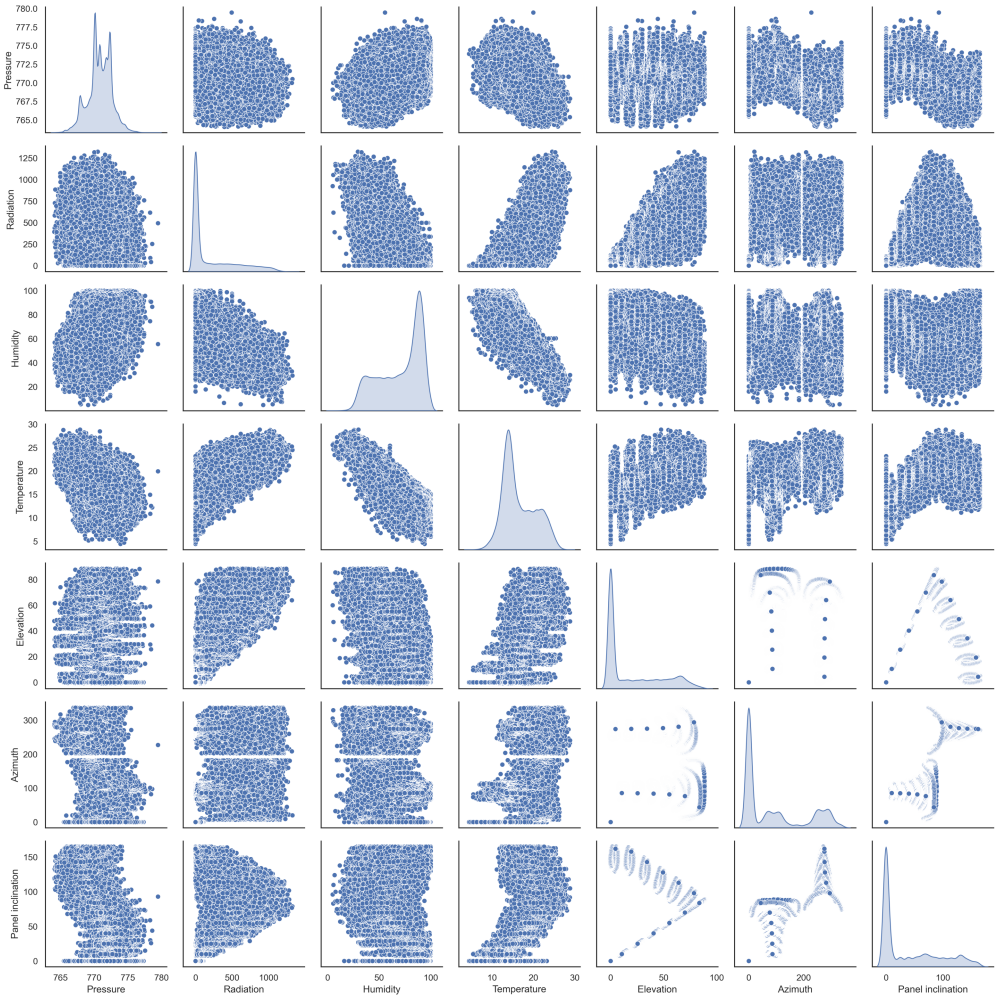

Figure 20: Scatter plots of the input and output data

Figure 21: Heat map of the dataset

4.2 Web interface

We chose to work with a combination of JavaScript and PHP to build the site, using the model-view-controller methodology. The data is stored in some tables inside a general database. Those tables collect the weather data, the electrical generation information, and the features about the sun position. That could be checked in the web interface, which shows the data in form of graphs.

REFERENCES

[1] D. D. Fiallos Chamorro, “Determinación del punto óptimo de potencia de paneles fotovoltaicos en base a variables difusas mediante el modelo de liu jordan,” B.S. thesis, 2020.

[2] G. B. Alexandra and P. G. Lucy, “Diseño e implementación de un sistema de paneles solares como prueba piloto para suministro energético de dispositivos móviles, en la universidad santo tomás, sede villavicencio campus loma linda,”

[3] D. A. Mejıa, I. T. Chávez, and A. Mejıa, “Positioning control of square arrangements of solar panels by solar tracing using fuzzy logic,” *South Florida Journal of Development*, vol. 2, no. 2, pp. 3318–3331, 2021.

[4] F. I. Mustafa, S. Shakir, F. F. Mustafa, and A. T. Naiyf, “Simple design and implementation of solar tracking system two axis with four sensors for baghdad city,” in *2018 9th International Renewable Energy Congress (IREC)*, IEEE, 2018, pp. 1–5.

[5] M. M. REYES MERO, S. TUÁREZ, and I. FERNANDO, “Análisis comparativo técnico-económico entre paneles solares estáticos y paneles con sistema de seguimiento de dos ejes instalados en la ciudad de manta-uleam.,” Ph.D. dissertation, 2021.

[6] S. Seme, B. Štumberger, M. Hadžiselimović, and K. Sredenšek, “Solar photovoltaic tracking systems for electricity generation: A review,” *Energies*, vol. 13, no. 16, p. 4224, 2020.

[7] J. S. Fuentevilla, M. Ávalos, and D. Garcıa, “Diseño y construcción de un sistema de seguimiento fotovoltaico,” *Universidad Tecnológica de la Mixteca*, 2012.

[8] S. V. Arpi Puga and B. G. Prado Bermeo, “Diseño de un seguidor solar de doble eje para un sistema de energıa fotovoltaica en el centro de salud de la comunidad de yaapi,” B.S. thesis, 2022.

[9] F. Ordóñez, C. Morales, J. López-Villada, and S. Vaca, “Assessment of the energy gain of photovoltaic systems by using solar tracking in equatorial regions,” *Journal of Solar Energy Engineering*, vol. 140, no. 3, 2018.

[10] ENER. “Yingli solar yl250p-29b.” (2015), [Online]. Available: https://www.enerbrasil.com.br/loja/?p=111 (visited on 12/17/2022).

[11] SolarDesignTool. “Yingli solar yl250p-29b (250w) solar panel.” (2015), [Online]. Available: http://www.solardesigntool.com/components/module-panel-solar/Yingli-Solar/2147/YL250P-29b/specification-data-sheet.html (visited on 09/04/2022).

[12] J. A. P. López, A. L. Soto, F. B. Ramos, and B. G. Flores, “Comparativa de la eficiencia entre un sistema fotovoltaico con seguimiento solar y un sistema fotovoltaico fijo/-comparison between a photovoltaic solar tracker efficiency and a fixed photovoltaic system,” *CIBA Revista Iberoamericana de las Ciencias Biológicas y Agropecuarias*, vol. 7, no. 13, pp. 105–129, 2018.

[13] Rexroth. “Perfiles de soporte.” (2020), [Online]. Available: https://www.boschrexroth.com/ics/cat/content/assets/Online/do/Strut_profiles_MGE_14_ES_2019-07_20191202_160243.pdf (visited on 12/05/2022).

[14] MatWeb. “Aluminum 6061-t4; 6061-t451.” (2018), [Online]. Available: https://www.matweb.com/search/DataSheet.aspx?MatGUID=d5ea75577b1b49e8ad03caf007db5ba8&ckck=1 (visited on 12/05/2022).

[15] ——, “Aisi 1040 steel, as rolled.” (2018), [Online]. Available: https://www.matweb.com/search/DataSheet.aspx?MatGUID=c8ada14779744d008a6c3e80f035c5d5 (visited on 12/05/2022).

[16] J. E. Shigley, C. R. Mischke, F. P. Bocanegra, and C. O. Correa, “Diseño en ingeniería mecánica,” 1990.

[17] Metalmecanica-facil. “Cálculo del tornillo sin fin y su corona - (sistema métrico).” (2016), [Online]. Available: https://www.youtube.com/watch?v=8tA7yF3zIOE (visited on 12/08/2022).

[18] J. Santamaria. “Cálculo de engranajes.” (2015), [Online]. Available: https://www.youtube.com/watch?v=Ci2Hg7DvYYw (visited on 12/08/2022).

[19] L. Serna, F. Albán, *et al.*, “Ácido poliláctico (pla): Propiedades y aplicaciones,” *Ingeniería y competitividad*, vol. 5, no. 1, pp. 16–26, 2003.

[20] E. S. Villegas Tapia and L. E. Alcívar Tello, “Diseño de un sistema fotovoltaico para la escuela de educación básica simón bolívar en la comunidad masa 2, golfo de guayaquil,” B.S. thesis, 2020.

[21] S. de Ambiente del Municipio del Distrito Metropolitano Quito. “Datos historicos remmaq.” (2022), [Online]. Available: http://www.quitoambiente.gob.ec/index.php/descarga-datos-historicos (visited on 03/27/2022).

[22] SunEarthTools. “Calculation of sun’s position in the sky for each location on the earth at any time of day. azimuth, sunrise sunset noon, daylight and graphs of the solar path.” (2009), [Online]. Available: https://www.sunearthtools.com/dp/tools/pos%5C_sun.php (visited on 08/25/2022).